American Journal of Ophthalmology Case Reports 26 (2022) 101490

Contents lists available at ScienceDirect

American Journal of Ophthalmology Case Reports

journal homepage: www.ajocasereports.com/

Detailed analyses of microstructure of photoreceptor layer at different severities of occult macular dystrophy by ultrahigh-resolution SD-OCT

Kazushige Tsunoda [a,*], Gen Hanazono [a,b]

[a] Division of Vision Research, National Institute of Sensory Organs, National Hospital Organization Tokyo Medical Center, 2-5-1 Higashigaoka, Meguro-ku, Tokyo, 152-8902, Japan
[b] Higashimatsudo Hanazono Eye Clinic, 2-3-2 Higashimatsudo, Matsudo City, Chiba, 270-2225, Japan

ARTICLE INFO

Keywords:
Occult macular dystrophy
Photoreceptors
Optical coherence tomography
Ultrahigh-resolution OCT
Interdigitation zone
Ellipsoid zone

ABSTRACT

Purpose: To analyze the microstructures of the photoreceptor layer in detail in eyes with occult macular dystrophy (OMD, Miyake's disease) by ultrahigh-resolution spectral-domain optical coherence tomography (UHR-SD-OCT).

Observations: Twenty-eight normal subjects and 5 patients with OMD of different severities were studied. Cross-sectional images through the fovea were recorded with a UHR-SD-OCT system with a depth resolution of <2.0 μm. In patients with OMD, the UHR-SD-OCT images revealed abnormal photoreceptor microstructures which were not detected in the conventional SD-OCT images. The UHR-SD-OCT images showed that the interdigitation zone (IZ) was not present and the outer segments were hyperreflective with hyperreflective dots (HRDs) aligned like string of pearls during the earlier stages. There was a disruption of the ellipsoid zone (EZ) which appeared as clusters of larger HRDs, and these HRDs became less apparent with increasing time. The outer segments became hyporeflective and rod IZ became apparent with longer duration of the disease process.

Conclusions and Importance: The UHR-SD-OCT images show detailed characteristics of the photoreceptor microstructures of different severities during the progression of OMD. These detailed observations will help in understanding the mechanisms involved in the retinal pathology and should provide important information for their treatments.

1. Introduction

Improvements of the resolution of optical coherence tomographic (OCT) images have greatly contributed to the understanding of both the etiology and natural course of various retinal diseases. Detailed examinations of the photoreceptor microstructures are very important especially in inherited retinal diseases because it can provide important information not only for a correct diagnosis but also for the assessment of the severity and when therapy should begin. However, the axial resolution of the conventional spectral-domain (SD) OCT is 5–7 μm,[1] and there is a significant gap between what is observed in the diseased retina by the conventional OCT and what is happening structurally during the process of neuronal atrophy of diseased eyes.

Occult macular dystrophy (OMIM-613587) is a very slowly progressive macular dystrophy with normal funduscopic appearance.[2,3] Heterozygous missense variants in the *RP1L1* gene accounts for most of the cases, and those with mutations in the *RP1L1* gene are specifically called *RP1L1*-related macular dystrophy, or Miyake's disease.[4–6] Furthermore, patients carrying a missense mutation in one of the two hot spots, amino acid 45 in exon 2, or one of 8 amino acids (1194–1201) in exon 4, have been shown to have very similar OCT findings and clinical courses.[5–13] We have determined the course of the OMD disease process in detail in the largest multicenter cohort, and found that the severity in visual acuity reduction was correlated with the disease duration. We have proposed the clinical stages of OMD based on the findings of conventional SD-OCT.[7] However, due to the limited resolution of conventional SD-OCT, we could not determine the detailed structural changes during the process of photoreceptor atrophy.

An ultrahigh-resolution SD-OCT (UHR-SD-OCT; KOWA OCT Bi-μ; Kowa Company, Ltd., Japan) device was recently developed. It has an axial resolution of less than 2.0 μm which is about three-times better than the conventional SD-OCT, and obtained clearer images of the outer retinal structures both in normal eyes[14,15] and diseased eyes.[16,17] We have examined the B-scan images obtained by the UHR-SD-OCT device

* Corresponding author.
E-mail addresses: kazushige.tsunoda@kankakuki.jp (K. Tsunoda), hana@tkf.att.ne.jp (G. Hanazono).

https://doi.org/10.1016/j.ajoc.2022.101490
Received 24 November 2021; Received in revised form 5 March 2022; Accepted 13 March 2022
Available online 17 March 2022
2451-9936/© 2022 The Authors. Published by Elsevier Inc. This is an open access article under the CC BY-NC-ND license (http://creativecommons.org/licenses/by-nc-nd/4.0/).

of 28 normal eyes and 5 eyes with OMD whose etiologies were genetically confirmed. Because all the patients with *RP1L1*-related macular dystrophy are very slowly progressive, the assessments of longitudinal follow-up examinations for individual patients are not practical. Further, there is no histological study of the patients with *RP1L1*-related macular dystrophy. We have thus compared the UHR-SD-OCT data from patients at different disease durations and severities based on the classification we have established.[7] We have found many characteristic features of the changes in the photoreceptor microstructures that may occur during the process of photoreceptor damage by the examination of the high-resolution images of the cone interdigitation zone (IZ), rod IZ, and the hyperreflective dots (HRDs) of the ellipsoid zone (EZ) and outer segments. The information gained by the UHR-SD-OCT images will be helpful in filling the gap between the OCT imaging and histological studies not only for OMD but also for other retinal diseases.

2. Materials and methods

The procedures used in this study adhered to the tenets of the Declaration of Helsinki and were approved by the Ethics Committee of the National Institute of Sensory Organs, National Hospital Organization Tokyo Medical Center (Reference; R18-029). A signed informed consent was received from all of the subjects for the examinations used after an explanation of the nature and possible consequences of the study.

2.1. Participants

We examined 28 eyes from 28 normal controls including 10 men and 18 women whose mean ± SD age was 38.9 ± 9.5 years with a range of 22–65 years. None had significant refractive errors (hyperopia $> +2.0$ diopter or myopia < -6.0 diopter).

We also examined 5 patients with *RP1L1*-related OMD. The phenotype of these patients was determined by comprehensive ophthalmic examinations[5] including ophthalmoscopy, fundus photography, fundus autofluorescence, conventional SD-OCT (Cirrus HD OCT, version 6.5; Carl Zeiss Meditec, Dublin, CA, USA), and full-field electroretinography (ERG) (LE4000, Tomey Corporation, Aichi, Japan).[18]

Genetic analysis was performed on all the patients. To search for the causative genes, whole exome sequencing with targeted analysis for retinal disease-causing genes on RetNET (https://sph.uth.edu/retnet/home.htm) and inheritance filtration were performed as described in detail.[6] Some of the clinical and genetic data of these patients have been published elsewhere.[5–7] All 5 cases with OMD had a single heterozygous variant of the *RP1L1* gene (3 cases, c.133C>T, p.Asp45Trp; one case, c.3596C>G, p.Ser1199Cys; one case, c.3599G>A, p.Gly1200Asp).[6]

2.2. Ultrahigh resolution spectral domain optical coherence tomography (UHR-SD-OCT) imaging

An UHR-SD-OCT system (KOWA OCT Bi-μ; Kowa Company, Ltd., Japan) with a broadband superluminescent diode light source was used on all subjects.[14] The center wavelength of the light source was 860 nm, and the bandwidth was 135 nm. Each A-scan had a depth of 2.6 mm which was composed of 2048 pixels and allowed a digital depth sampling of 1.27 μm/pixel. Each B-scan spanned 30° and consisted of 1800 A-scans. For a 9.0 mm width image, the digital width sampling was 5 μm/pixel. Cross-sectional horizontal and vertical images with a 9.0 mm width across the fovea were recorded in all the subjects. Twenty consecutive line scans were averaged for each trial through un-dilated (controls) and dilated (patients) pupils.

To evaluate the microstructures of the outer retina, we measured the longitudinal reflectivity profiles (LRPs). For each LRP, the reflectivity was averaged over 16 pixels in width.

3. Results

3.1. UHR-SD-OCT images of normal eyes

Representative horizontal and vertical B-scan images across the fovea of a 41-year-old woman with normal eyes taken with the UHR-SD-OCT device are presented together with the LRPs (Fig. 1). Due to the higher axial resolution, hyperreflective regions were present which were not mentioned in the International Nomenclature for Optical Coherence Tomography [IN•OCT],[19] viz., Bruch's membrane (Fig. 1C and F), rod IZ (Fig. 1B, C, 1E, and 1F), and dot-like regions with hyperreflectivity between the EZ and cone IZ (Fig. 2). The hyperreflective band of the rod IZ was clearly distinguishable from the RPE in 21 of 28 normal eyes (75%). In the 7 eyes in which the rod IZ was not distinguishable from the RPE in the B-scan images, the LRP showed a clear peak of high reflectivity between the cone IZ and the RPE/Bruch membrane in all of these eyes (Fig. 1C and F).

The expanded B-scan images of normal eyes showed that there were distinctly observed dot-like hyperreflective regions between the EZ and cone IZ (Fig. 2B and D, black and yellow arrows). In the conventional OCTs, this region appeared to be hyporeflective and was identified as the outer segments of the photoreceptors by the IN•OCT.[19]

3.2. Changes in photoreceptor microstructures with different severities of OMD

The B-scan images of five eyes of five cases of OMD taken by a UHR-SD-OCT are shown in Fig. 3A to E, and one B-scan image of the same eye in Fig. 3C taken by a conventional SD-OCT is shown in Fig. 3F for comparison. According to the clinical stages based on the visual symptoms and OCT findings, Case A was classified as Stage Ia and Cases B to E were classified as Stage IIb.[7] The five cases are presented according to the severity of foveal atrophy and the BCVA from mild to severe.

The OCT images of the left eye of a 53-year-old woman whose BCVA was 20/25 are shown in Fig. 3A. The EZ is blurred and cone IZ is disrupted at the fovea (Fig. 3A, white arrowhead). However, both the EZ and the cone IZ are normal at the parafovea (Fig. 3A, yellow arrows). In the more peripheral regions, the EZ appears mildly disrupted with clusters of hyperreflective dots (HRDs) (Fig. 3A, yellow arrowhead) and the cone IZ could not be seen. Instead, there were HRDs in the outer segment layer that appeared like string of pearls, *i.e.*, HRDs consecutively aligned in a line perpendicular to the RPE (Fig. 3A, yellow asterisk).

The OCT images of the right eye of a 36-year-old man whose BCVA was 20/50 are shown in Fig. 3B. The arch-shaped region of blurred EZ at the fovea is expanded laterally more than in Case A (Fig. 3B, white arrowhead), and HRDs are observed at the location of the outer segments (Fig. 3B, right most yellow arrowhead). The EZ and cone IZ are seen as in normal eyes in the peri-macular region (Fig. 3B, yellow arrows), but in the macular region, the EZ appeared disrupted with clusters of HRDs (Fig. 3B, left most three yellow arrowheads) and the cone IZ was not visible.

The OCT images of the left eye of a 39-year-old man whose BCVA was 20/63 are shown in Fig. 3C. The arch-shaped region of a blurred EZ at the fovea is expanded laterally more than that in Case B, and the normal appearing ELM passes through it (Fig. 3C, white arrowhead). The cone IZ is not present in the entire macular region and the EZ appears disrupted with clusters of HRDs (Fig. 3C, yellow arrowheads). The outer segments appear like string of pearls similar to that in Fig. 3A (Fig. 3C, yellow asterisk).

The OCT images of the left eye of a 22-year-old woman whose BCVA was 20/125 are shown in Fig. 3D. There is an arch-shaped region of blurred EZ at the fovea, and the normal appearing ELM passes through it (Fig. 3D, white arrowhead). The EZ appears disrupted with clusters of HRDs (Fig. 3D, yellow arrowheads). The outer segments appear more hyporeflective than in Cases A to C and the string-of-pearl-like structures

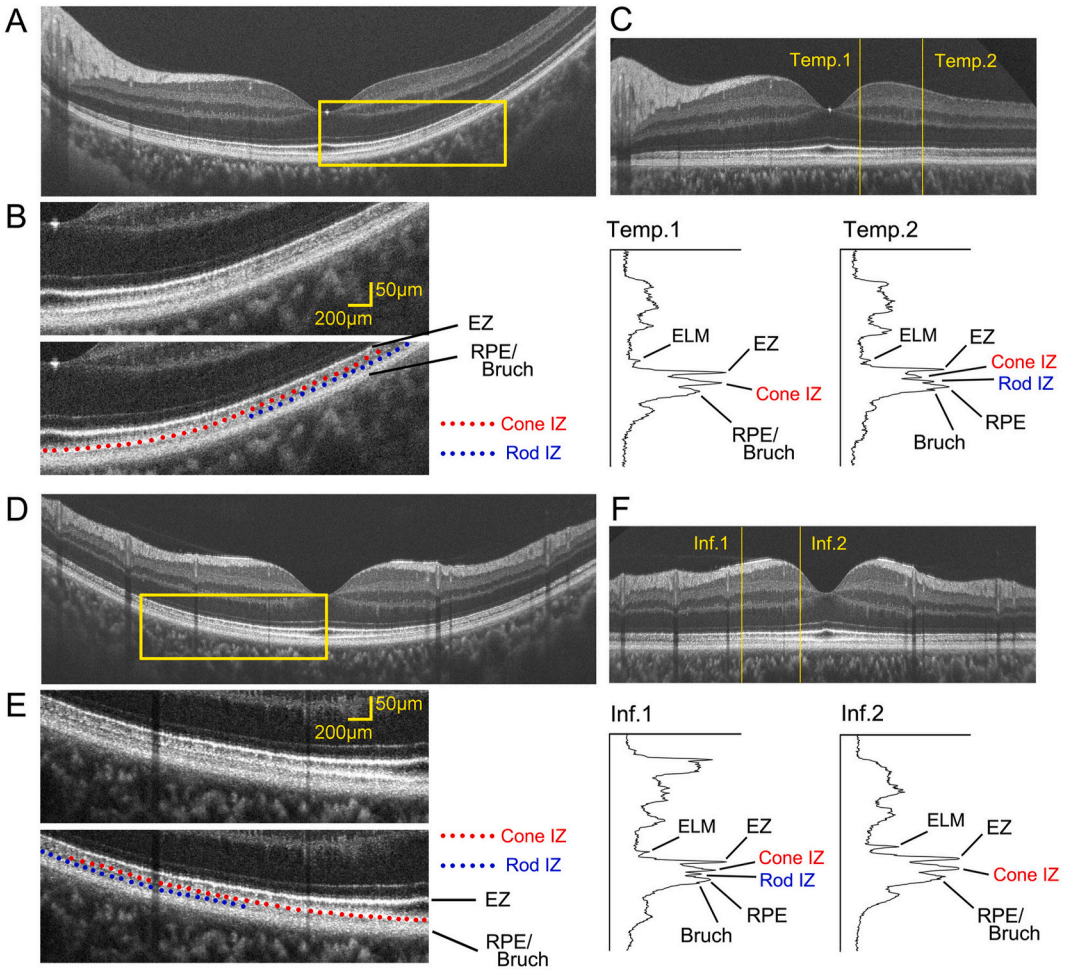

Fig. 1. Ultrahigh-resolution SD-OCT (UHR-SD-OCT) image of a normal eye. **A.** Horizontal B-scan image across the fovea of a 41-year-old woman taken by a UHR-SDR-OCT device. **B.** Expanded image of the yellow rectangle in A. Locations of both the cone and rod interdigitation zone (IZ) are shown by red and blue dotted lines, respectively. **C.** Longitudinal reflectivity profiles (LRP) in the regions indicated by the yellow arrows on the flattened OCT image. Rod IZ is seen as a distinct hyperreflective peak between the cone IZ and RPE/Bruch's membrane in Temp. 2 but not in Temp.1. **D.** Vertical B-scan image across the fovea of the same subject in A, taken by UHR-SDR-OCT. **E.** Expanded image of the yellow rectangle in D. Locations of both the cone and rod IZs are shown by red and blue dotted lines, respectively. **F.** The LRP in the regions indicated by the yellow arrows on the flattened OCT image. The rod IZ is seen as a distinct hyperreflective peak between the cone IZ and RPE/Bruch's membrane in Inf.1, but not in Inf.2. ELM = external limiting membrane; EZ = ellipsoid zone of photoreceptor; IZ = interdigitation zone of photoreceptor; RPE = retinal pigment epithelium. Temp. = temporal; Inf. = inferior. . (For interpretation of the references to colour in this figure legend, the reader is referred to the Web version of this article.)

were not detected.

The OCT images of the right eye of a 51-year-old woman whose BCVA was 20/200 are shown in Fig. 3E. The cone IZ is not present in the entire macular region and the EZ appears blurred and hyporeflective with a smaller number of HRDs than in Cases A to D (Fig. 3E, yellow arrowhead). The outer segments appeared to be hyporeflective and the rod IZ is clearly observed above the RPE (Fig. 3E, yellow arrow).

Fig. 4 shows the LRPs of a normal eye in Fig. 1, and cases with OMD shown in Fig. 3B and E. In the case shown in Fig. 3B, the peak of EZ appears high and sharp in Inf. 1, but lower and broader in Inf. 2. The peak of Cone IZ does not appear in Inf. 2 (Fig. 4B). In the more advanced case shown in Fig. 3E, the peak of the EZ appears to be lower and broader both in Inf. 1 and 2, and the peak of the cone IZ does not appear either in Inf. 1 or 2 (Fig. 4C). There is a peak of the rod IZ in Inf. 1.

4. Discussion

4.1. Process of cone photoreceptor damage in cases with OMD

In the early stage with mild visual disturbance, the conventional SD-OCT had already shown that the EZ was blurred and the cone IZ was not visible at the fovea. With time, the region of abnormality in the EZ and cone IZ expanded toward the periphery.[5,7,12]

The UHR-SD-OCT images of normal eyes revealed that the outer segment region between the two distinct EZ and cone IZ bands was not simply hyporeflective, but dot-like regions with hyperreflectivity were sparsely distributed between the EZ and cone IZ (Fig. 2B and D, black and yellow arrows). These dot-like regions were also observed in diseased eyes as HRDs, but they may represent something different between normal eyes and diseased eyes. The dot-like regions in normal eyes may represent minimally abnormal or physiological changes among the normal structures of the outer segment, or an optical artifact which was induced by occasionally misaligned structures of the normal outer segments.

In the earlier stages of OMD, the band of the cone IZ was not detected, and the HRDs were more distinctly observed in the location of the outer segments. The HRDs were consecutively aligned and appeared like a string of pearls (Fig. 3A and C, yellow asterisk). In the advanced stage, the string-of-pearl-like structures could not be observed, and the outer segments appeared more hyporeflective (Fig. 3D and E). Instead,

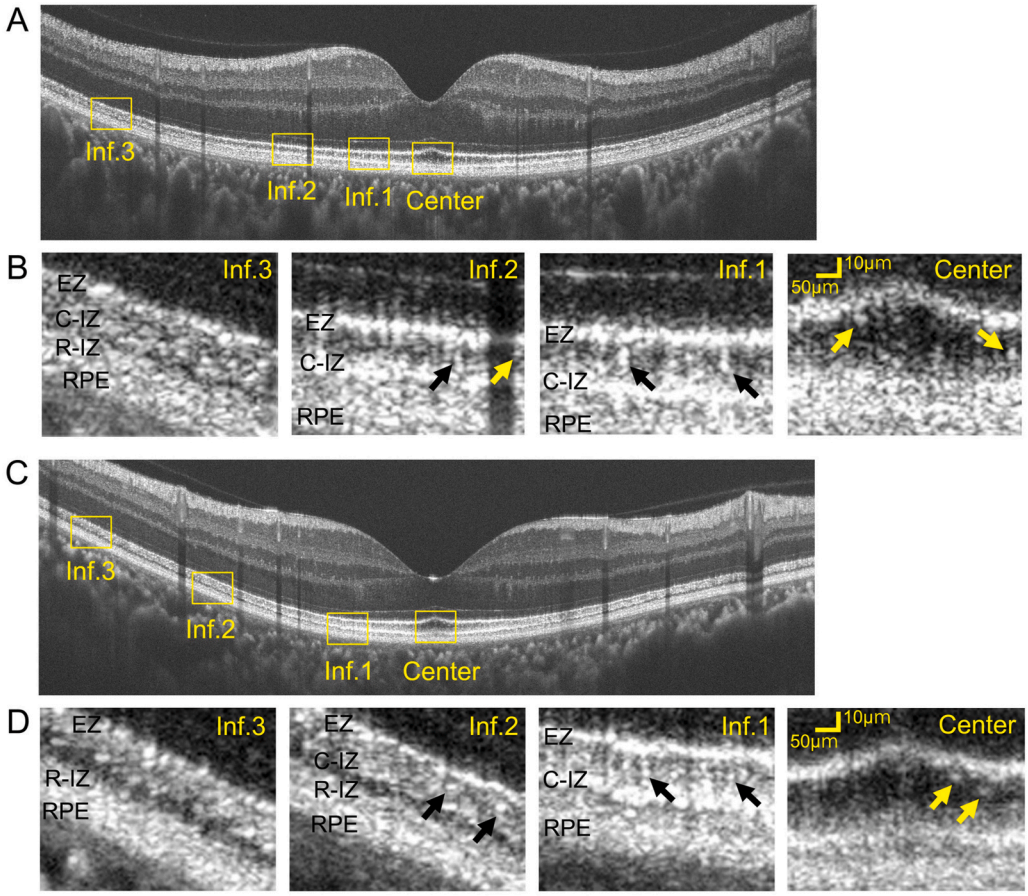

Fig. 2. Small dot-like regions with hyperreflectivity in the outer segments between the EZ and cone IZ in normal eyes. **A.** Vertical B-scan image across the fovea of a 31-year-old man with normal eyes taken by UHR-SDR-OCT. **B.** Expanded image of the yellow rectangles in A. **C.** Vertical B-scan image across the fovea of a 40-year-old woman with normal eyes taken by UHR-SDR-OCT. **D.** Expanded image of the yellow rectangles in C. Small dot-like regions with hyperreflectivity are observed between the EZ and cone IZ (Fig. 2B and D, black and yellow arrows). They are independent of the highly reflective EZ and cone IZ. EZ = ellipsoid zone of photoreceptors; C-IZ = cone interdigitation zone of photoreceptors; R-IZ = rod interdigitation zone of photoreceptors; RPE = retinal pigment epithelium; Inf. = inferior. . (For interpretation of the references to colour in this figure legend, the reader is referred to the Web version of this article.)

the rod IZ was clearly observed above the RPE (Fig. 3E, yellow arrow).

There was another type of larger HRDs in the region of EZ in the OMD eyes, *i.e.*, part of the disrupted EZ appeared as clusters of HRDs (Fig. 3A to E, yellow arrowheads). The clusters of HRDs were more distinctly observed in the earlier stages (Fig. 3A to D, yellow arrowheads). In the advanced stage, the EZ appeared blurred with fewer HRDs (Fig. 3E).

In the foveal region, the EZ was blurred without HRDs from the early stage, and the width of the blurred EZ expanded laterally during the course of the disease process (Fig. 3A to E, white arrowheads). There was an atrophy of both the inner and outer segments of the photoreceptors in Miyake's disease due to a dysfunction of the connecting cilia.[4,20,21] Although the cone IZ was not detected and the EZ became blurred, the space between the EZ and RPE was preserved in the later stages of OMD (Fig. 3).[5,7] This is a characteristic nature of OMD in which only the cone photoreceptors in the macular region are affected and rod photoreceptors are normally preserved until the late stage.[3] In the late stage, the rod IZ was clearly observed (Fig. 3E, yellow arrow) and the blurred EZ without the HRDs may represent the 'rod EZ', and it includes only the ellipsoids of the rod photoreceptors.

4.2. Origin of hyperreflective dots in UHR-SD-OCT images

The HRDs, which were observed in diseased eyes, were located independently from the highly reflective bands of the EZ and cone IZ, and thus, they are neither speckle noise nor optical artifacts derived from the high-intensity signals.[22] They possibly represent some anatomical components of the cone or rod photoreceptors.

The HRDs in the outer segments of the photoreceptors may be packets of abnormal outer segment disks which have changed their orientation in the process of phagocytosis, or they may be phagosomes being phagocytosed by the apical processes of the RPE just below the outer segment tips.[23,24] We suggest that abnormal phagocytosis of the outer segments during the disease process produced the cluster of rotated packets of outer segment disks which had abnormal hyperreflectivity in the outer segment region. The HRDs may also be attributed to the increased reflectivity of the outer segments alone due to mechanical stress[25] or degenerative changes.[26]

The possible source of the HRDs in the EZ band, which appeared larger than those in the outer segments, could be abnormal ellipsoid fragments in the inner segment of the photoreceptors that have lost their connection with the normal outer segments. They may not contain normally functioning mitochondria and then undergo apoptosis. The results of a histological study by Litts et al. showed that during the process of atrophy, the mitochondria of the ellipsoids redistribute toward the nucleus, and the inner segment of the cones appear broadened.[27] The cluster of large HRDs and thickened EZ in the fovea of OMD[5,7] (Fig. 3, white arrowheads) may result from an expansion of the ellipsoid region containing mitochondria during the process of atrophy. Further, the clusters of HRDs in Fig. 3B are thicker than those in Fig. 3C. This may reflect a characteristic process of cellular damage of the photoreceptor ellipsoid but its mechanism is unknown.

The horizontal diameter of the HRDs in the disrupted EZ was approximately 16 μm and that of the HRDs in the outer segment was approximately 12 μm (Fig. 3) The horizontal diameter of HRDs was much larger than that of the normal cone inner segments in the paramacular regions (approx. 7 μm) or the cone outer segments at the fovea (approx. 1–2 μm).[28,29] Thus, both the HRDs in the disrupted EZ and outer segment observed in the UHR-SD-OCT images most likely do not represent individual photoreceptors but clusters of cone elements, or abnormally expanded individual cone photoreceptors. In either case, the HRDs observed during the course of OMD surely represent the process of

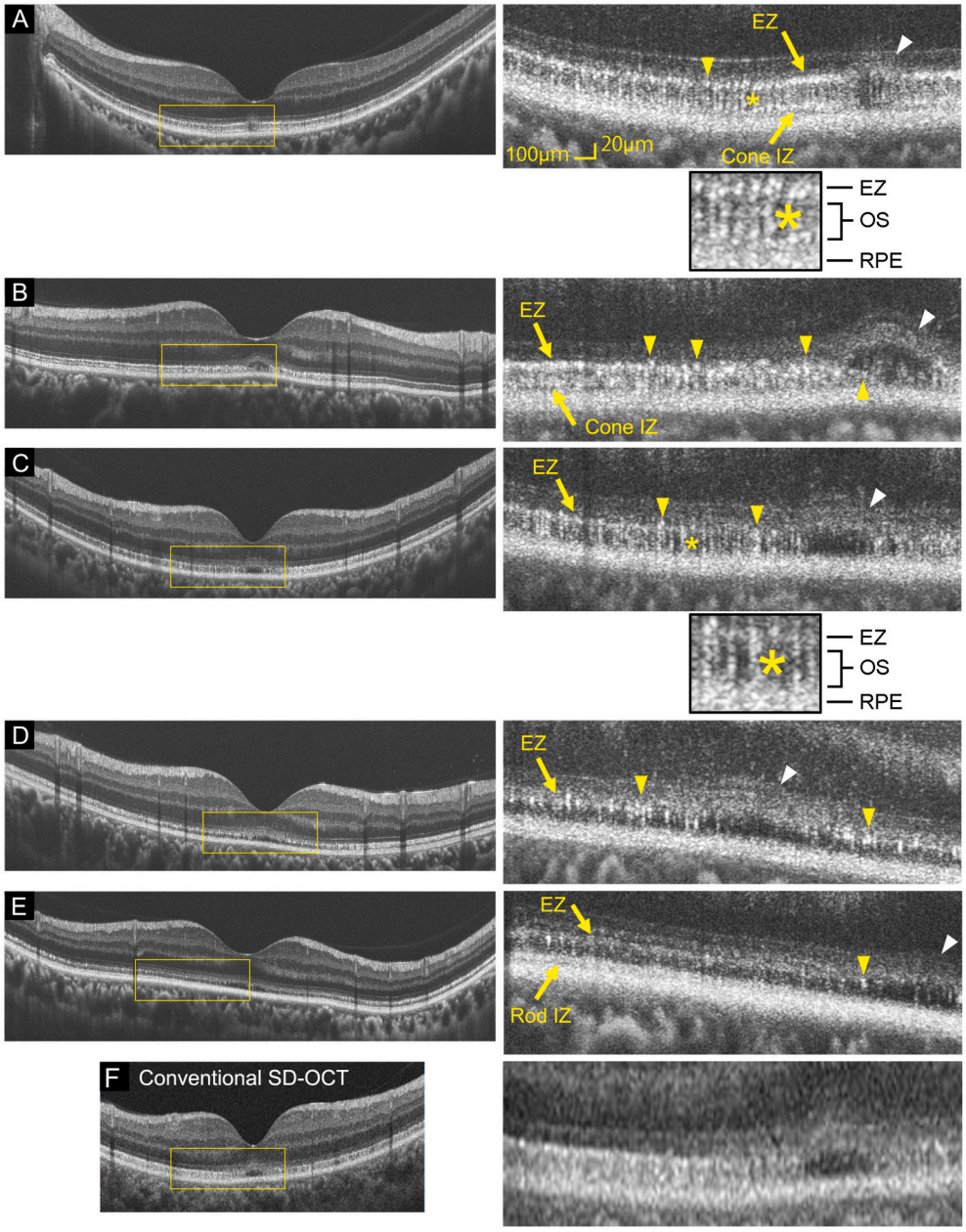

Fig. 3. B-scan images of five eyes in five cases with OMD listed according to the severity of visual acuity and photoreceptor atrophy from mild to severe. **A.** Horizontal B-scan image of the left eye of a 53-year-old woman whose decimal best-corrected visual acuity (BCVA) was 20/25. In the expanded image, the EZ is blurred and the cone IZ is disrupted at the fovea (white arrowhead). Both the EZ and cone IZ are normal only at the parafovea (yellow arrows). In the more peripheral region, the EZ appears slightly disrupted with clusters of hyperreflective dots (HRDs) (yellow arrowhead) and the cone IZ is not present. There are HRDs in the outer segment consecutively aligned in a line that appear like string of pearls (yellow asterisk). The expanded image (2x) of the string of pearls is shown below. **B.** Vertical B-scan image of the right eye of a 36-year-old man whose BCVA was 20/50. In the expanded image, the arch-shaped region of blurred EZ at the fovea is expanded laterally more than in Case A (white arrowhead), and HRDs are observed in the location of the outer segments (right-most yellow arrowhead). The EZ and cone IZ are normally observed in the peri-macular region (yellow arrows), but in the macular region, the EZ appears disrupted with cluster of HRDs (left-most three yellow arrowheads) and the cone IZ is not visible. **C.** Vertical B-scan image of the left eye of a 39-year-old man whose BCVA was 20/63. In the expanded image, the arch-shaped region of blurred EZ at the fovea is expanded laterally more than that in Case B, and the normal appearing ELM passes through it (white arrowhead). The cone IZ is not present in the entire macular region and the EZ appears disrupted with clusters of HRDs (yellow arrowheads). The outer segments appear like string of pearls (yellow asterisk). The expanded image (2x) of the string of pearls is shown below. **D.** Vertical B-scan image of the left eye of a 22-year-old woman whose BCVA was 20/125. In the expanded image, there is arch-shaped region of blurred EZ at the fovea, and the normal appearing ELM passes through it (white arrowhead). The cone IZ is not present in the entire macular region and the EZ appears disrupted with clusters of HRDs (yellow arrowheads). The outer segments appear more hyporeflective than in Cases A to C and the string-of-pearl-like structures are not present. **E.** Vertical B-scan image of the right eye of a 51-year-old woman whose BCVA was 20/200. In the expanded image, there is arch-shaped region of blurred EZ at the fovea (white arrowhead). The cone IZ is not observed in the entire macular region and the EZ appears blurred and hyporeflective with smaller number of HRDs than in Cases A to D (yellow arrowhead). The outer segments appear more hyporeflective than in cases A to C, and the rod IZ is clearly observed above the RPE (yellow arrow). **F.** Vertical B-scan images of the same eye as in C taken by a conventional SD-OCT. EZ = ellipsoid zone of photoreceptor; IZ = interdigitation zone of photoreceptor; OS = outer segment; RPE = retinal pigment epithelium.. (For interpretation of the references to colour in this figure legend, the reader is referred to the Web version of this article.)

photoreceptor damage, which could not be detected by the conventional SD-OCT devices.

HRDs are round-shaped hyperreflective region which become apparent in the UHR-SD-OCT images, and the difference with hyper reflective foci (HRFs) should be discussed. HRFs are focal, hyperreflective lesions detected by SD-OCT in various types of retinal disorders, e.g., diabetic retinopathy,[30] age-related macular degeneration,[31] and hereditary retinal diseases such as Stargardt disease,[32] retinitis pigmentosa,[26,33] vitelliform lesions of the macula,[34,35] and choroideremia.[36] The HRFs in inherited retinal diseases have been suggested to originate from microglia, RPE cells, or both in the degenerated retina, and they represent pathological processes of the diseases. On the other hand, the size of the HRDs in our cases were much smaller than that of HRF and could not be observed by the conventional SD-OCTs. Small dot-like regions with hyperreflectivity between the EZ and cone IZ were also observed even in the normal retinas (Fig. 2B and D, yellow and

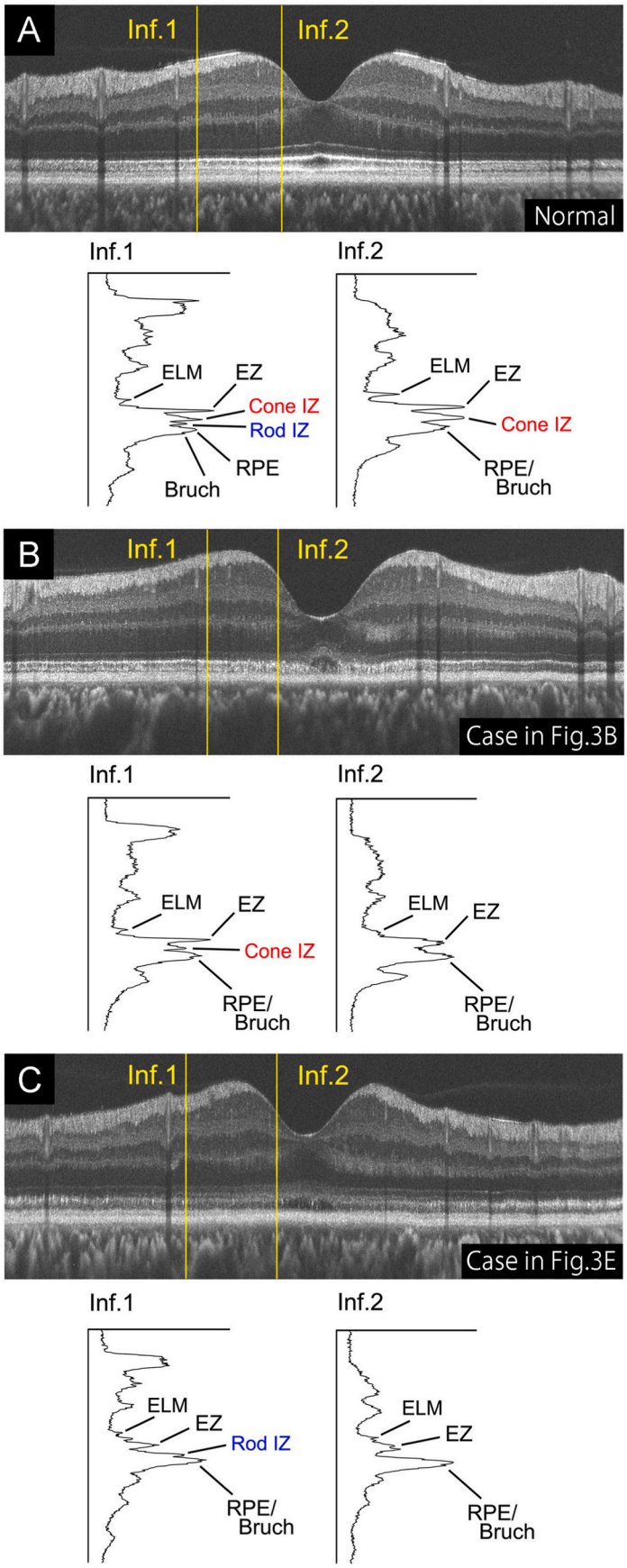

Fig. 4. Longitudinal reflectivity profiles (LRPs) of a normal eye in Fig. 1, and Cases with OMD shown in Fig. 3B and E. **A.** Longitudinal reflectivity profiles (LRP) of a normal eye in Fig. 1 in the regions indicated by yellow arrows on the flattened OCT image. The EZ and Cone IZ have high and sharp peaks both in the locations of Inf. 1 and 2. **B.** LRPs of the case with OMD in Fig. 3B. The peak of the EZ appears high and sharp in Inf. 1, but lower and broader in Inf. 2. The peak of the Cone IZ does not appear in Inf. 2. C. LRPs of more advanced case with OMD in Fig. 3E. The peak of EZ appears lower and broader both in Inf. 1 and 2. The peak of Cone IZ does not appear either in Inf. 1 or 2. ELM = external limiting membrane; EZ = ellipsoid zone of photoreceptor; IZ = interdigitation zone of photoreceptor; RPE = retinal pigment epithelium. Temp. = temporal; Inf. = inferior. . (For interpretation of the references to colour in this figure legend, the reader is referred to the Web version of this article.)

black arrows). Although the cellular origin of HRDs is unknown and is different from that of HRF, examinations of the HRDs in diseased retinas should provide more detailed information on the disease stages in various types of retinal disorders.

4.3. Limitations

Our study has several limitations. First, our study was retrospective and cross-sectional due to too slow progression of OMD.[5,7] However, the data of longitudinal follow-up examinations for 10–20 years will provide more accurate information of the disease processes. Second, we have selected patients with the same genetic abnormalities because the genotype difference in the same gene may cause different courses and severities in the OMD.[6,37] However, to investigate the general mechanism of photoreceptor damage in more detail, data from a wider variety of diseases of known etiology should be examined.

5. Conclusions

The UHR-SD-OCT device can obtain images that show the principal outer retinal structures of normal eyes which are not observed by the conventional SD-OCT. In addition, it can also record images that show detailed structural changes of these elements during the process of OMD. These detailed observations will help us understand the pathological mechanism(s) of other retinal dystrophies in general and provide important information for their therapeutic strategies.

Patient consent

This report does not contain any personal information that could lead to the identification of the patient. Written informed consent for the research was obtained from the patients prior to participation.

Acknowledgements and disclosures

Grant information

This study was supported by research grants from the 'National Hospital Organization Network Research Fund (H30–NHO-Sensory Organs-03 to KT)' and 'Health and Labour Sciences Research Grant for research on intractable diseases from Ministry of Health, Labour and Welfare of Japan (21K09712) to KT'.

The authors have no proprietary or commercial interest in any materials discussed in this article.

Meeting presentation

None.

Declaration of competing interest

K.T.: Payment for lectures - Santen Pharmaceutical Co., Ltd., Novartis Pharma Co., Ltd., Kowa Company, Ltd., and Senju Pharmaceutical Co., Ltd. Receipt of equipment - Kowa Company, Ltd.

G.H.: None.

The funding sources had no role in the design and conduct of this study; collection, management, analysis, interpretation of the data; preparation, review, or approval of the manuscript; and decision to submit the manuscript for publication.

We thank all the subjects for participation in this study. We thank Masaharu Mizouchi of Kowa Company for technical support. We thank our collaborators, Takeshi Iwata and Kaoru Fujinami of the National Institute of Sensory Organs for their contributions in genetic analysis of the patients. We also thank Professor Emeritus Duco Hamasaki of the Bascom Palmer Eye Institute, University of Miami School of Medicine, Miami, FL for editing our manuscript.

References

1. Drexler W, Fujimoto JG. State-of-the-art retinal optical coherence tomography. *Prog Retin Eye Res*. 2008;27:45–88.
2. Miyake Y, Ichikawa K, Shiose Y, Kawase Y. Hereditary macular dystrophy without visible fundus abnormality. *Am J Ophthalmol*. 1989;108:292–299.
3. Miyake Y, Horiguchi M, Tomita N, et al. Occult macular dystrophy. *Am J Ophthalmol*. 1996;122:644–653.
4. Akahori M, Tsunoda K, Miyake Y, et al. Dominant mutations in RP1L1 are responsible for occult macular dystrophy. *Am J Hum Genet*. 2010;87:424–429.
5. Tsunoda K, Usui T, Hatase T, et al. Clinical characteristics of occult macular dystrophy in family with mutation of Rp1l1 gene. *Retina-the J. Retin. Vit. Dis.* 2012;32:1135–1147.
6. Fujinami K, Kameya S, Kikuchi S, et al. Novel RP1L1 variants and genotype-photoreceptor microstructural phenotype Associations in cohort of Japanese patients with occult macular dystrophy. *Invest Ophthalmol Vis Sci*. 2016;57:4837–4846.
7. Nakamura N, Tsunoda K, Mizuno Y, et al. Clinical stages of occult macular dystrophy based on optical coherence tomographic findings. *Invest Ophthalmol Vis Sci*. 2019;60:4691–4700.
8. Ahn SJ, Cho SI, Ahn J, Park SS, Park KH, Woo SJ. Clinical and genetic characteristics of Korean occult macular dystrophy patients. *Invest Ophthalmol Vis Sci*. 2013;54:4856–4863.
9. Ziccardi L, Giannini D, Lombardo G, et al. Multimodal approach to monitoring and investigating cone structure and function in an inherited macular dystrophy. *Am J Ophthalmol*. 2015;160:301–312 e6.
10. Zobor D, Zobor G, Hipp S, et al. Phenotype variations caused by mutations in the RP1L1 gene in a large mainly German cohort. *Invest Ophthalmol Vis Sci*. 2018;59:3041–3052.
11. Ahn SJ, Ahn J, Park KH, Woo SJ. Multimodal imaging of occult macular dystrophy. *JAMA ophthalmol*. 2013;131:880–890.
12. Kato Y, Hanazono G, Fujinami K, et al. Parafoveal photoreceptor abnormalities in asymptomatic patients with RP1L1 mutations in families with occult macular dystrophy. *Invest Ophthalmol Vis Sci*. 2017;58:6020–6029.
13. Fujinami K, Yang L, Joo K, et al. Clinical and genetic characteristics of east asian patients with occult macular dystrophy (Miyake disease): east asia occult macular dystrophy studies report number 1. *Ophthalmology*. 2019;126:1432–1444.
14. Matsui Y, Kondo M, Uchiyama E, Mityata R, Matsubara H. New clinical ultrahigh-resolution SD-OCT using A-scan matching algorithm. In: *Graefe's archive for clinical and experimental ophthalmology = Albrecht von Graefes Archiv fur klinische und experimentelle Ophthalmologie*. 257. 2019:255–263.
15. Matsui Y, Miyata R, Uchiyama E, Matsubara H, Kondo M. Misalignment of foveal pit and foveal bulge determined by ultrahigh-resolution SD-OCT in normal eyes. Graefe's archive for clinical and experimental ophthalmology = Albrecht von Graefes Archiv fur klinische und experimentelle Ophthalmologie. 2020;258:2131–2139.
16. Cideciyan AV, Jacobson SG. Leber congenital amaurosis (LCA): potential for improvement of vision. *Invest Ophthalmol Vis Sci*. 2019;60:1680–1695.
17. Peshenko IV, Cideciyan AV, Sumaroka A, et al. A G86R mutation in the calcium-sensor protein GCAP1 alters regulation of retinal guanylyl cyclase and causes dominant cone-rod degeneration. *J Biol Chem*. 2019;294:3476–3488.
18. McCulloch DL, Marmor MF, Brigell MG, et al. ISCEV Standard for full-field clinical electroretinography (2015 update). *Doc Ophthalmol*. 2015;130:1–12.
19. Staurenghi G, Sadda S, Chakravarthy U, Spaide RF. Proposed lexicon for anatomic landmarks in normal posterior segment spectral-domain optical coherence tomography: the IN*OCT consensus. *Ophthalmology*. 2014;121:1572–1578.
20. Conte I, Lestingi M, den Hollander A, et al. Identification and characterisation of the retinitis pigmentosa 1-like1 gene (RP1L1): a novel candidate for retinal degenerations. *Europ.j.uman genet. : EJHG*. 2003;11:155–162.
21. Yamashita T, Liu J, Gao J, et al. Essential and synergistic roles of RP1 and RP1L1 in rod photoreceptor axoneme and retinitis pigmentosa. *J Neurosci*. 2009;29:9748–9760.
22. Zhang T, Kho AM, Srinivasan VJ. Improving visible light OCT of the human retina with rapid spectral shaping and axial tracking. *Biomed Opt Express*. 2019;10:2918–2931.
23. Steinberg RH, Wood I, Hogan MJ. Pigment epithelial ensheathment and phagocytosis of extrafoveal cones in human retina. *Philos Trans R Soc Lond Ser B Biol Sci*. 1977;277:459–474.
24. Anderson DH, Fisher SK, Steinberg RH. Mammalian cones: disc shedding, phagocytosis, and renewal. *Invest Ophthalmol Vis Sci*. 1978;17:117–133.
25. Scharf JM, Hilely A, Preti RC, et al. Hyperreflective stress lines and macular holes. *Invest Ophthalmol Vis Sci*. 2020;61:50.
26. Nagasaka Y, Ito Y, Ueno S, Terasaki H. Number of hyperreflective foci in the outer retina correlates with inflammation and photoreceptor degeneration in retinitis pigmentosa. *Ophthalmol. Retina*. 2018;2:726–734.
27. Litts KM, Messinger JD, Freund KB, Zhang Y, Curcio CA. Inner segment remodeling and mitochondrial translocation in cone photoreceptors in age-related macular degeneration with outer retinal tubulation. *Invest Ophthalmol Vis Sci*. 2015;56:2243–2253.
28. Curcio CA, Allen KA. Topography of ganglion cells in human retina. *J Comp Neurol*. 1990;300:5–25.
29. Liu J, Jung H, Dubra A, Tam J. Cone photoreceptor cell segmentation and diameter measurement on adaptive optics images using circularly constrained active contour model. *Invest Ophthalmol Vis Sci*. 2018;59:4639–4652.

30. Bolz M, Schmidt-Erfurth U, Deak G, Mylonas G, Kriechbaum K, Scholda C. Optical coherence tomographic hyperreflective foci: a morphologic sign of lipid extravasation in diabetic macular edema. *Ophthalmology*. 2009;116:914–920.
31. Framme C, Wolf S, Wolf-Schnurrbusch U. Small dense particles in the retina observable by spectral-domain optical coherence tomography in age-related macular degeneration. *Invest Ophthalmol Vis Sci*. 2010;51:5965–5969.
32. Piri N, Nesmith BL, Schaal S. Choroidal hyperreflective foci in Stargardt disease shown by spectral-domain optical coherence tomography imaging: correlation with disease severity. *JAMA ophthalmol.* 2015;133:398–405.
33. Kuroda M, Hirami Y, Hata M, Mandai M, Takahashi M, Kurimoto Y. Intraretinal hyperreflective foci on spectral-domain optical coherence tomographic images of patients with retinitis pigmentosa. *Clin Ophthalmol*. 2014;8:435–440.
34. Chen KC, Jung JJ, Curcio CA, et al. Intraretinal hyperreflective foci in acquired vitelliform lesions of the macula: clinical and histologic study. *Am J Ophthalmol.* 2016;164:89–98.
35. Parodi MB, Romano F, Sacconi R, et al. Intraretinal hyperreflective FOCI IN best vitelliform macular dystrophy. *Retina.* 2018;38:2379–2386.
36. Romano F, Arrigo A, MacLaren RE, et al. Hyperreflective FOCI as a pathogenetic biomarker IN choroideremia. *Retina.* 2020;40:1634–1640.
37. Kikuchi S, Kameya S, Gocho K, et al. Cone dystrophy in patient with homozygous RP1L1 mutation. *BioMed Res Int.* 2015;2015:545243.